Published in final edited form as:
J Biomech. 2012 February 23; 45(4): 660–665. doi:10.1016/j.jbiomech.2011.12.013.

ACUTE MECHANICAL EFFECTS OF ELASTASE ON THE INFRARENAL MOUSE AORTA: IMPLICATIONS FOR MODELS OF ANEURYSMS

M.J. Collins[1], **J.F. Eberth**[2,3], **E. Wilson**[4], and **J.D. Humphrey**[5]

[1]Department of Biomedical Engineering Texas A&M University, College Station, TX, USA

[2]Department of Engineering Technology University of Houston, Houston, TX, USA

[3]The Methodist Hospital Research Institute, Houston, TX, USA

[4]Department of Systems Biology and Translational Medicine Texas A&M Health Science Center, College Station, TX, USA

[5]Department of Biomedical Engineering and Vascular Biology and Therapeutics Program Yale University, New Haven, CT, USA

Abstract

Intraluminal exposure of the infrarenal aorta to porcine pancreatic elastase represents one of the most commonly used experimental models of the development and progression of abdominal aortic aneurysms. Morphological and histological effects of elastase on the aortic wall have been well documented in multiple rodent models, but there has been little attention to the associated effects on mechanical properties. In this paper, we present the first biaxial mechanical data on, and associated nonlinear constitutive descriptors of, the effects of elastase on the infrarenal aorta in mice. Quantification of the dramatic, acute effects of elastase on wall behavior in vitro is an essential first step toward understanding the growth and remodeling of aneurysms in vivo, which depends on both the initial changes in the mechanics and the subsequent inflammation-mediated turnover of cells and extracellular matrix that contributes to the evolving mechanics.

Keywords

stress; mechanics; constitutive relation; stiffness; elastin

Introduction

Abdominal Aortic Aneurysms (AAAs) are currently the 13th leading cause of death in the United States, but their impact on death and disability is expected to increase further in our aging population. For this reason, there has been a heightened interest over the past 15 to 20

Address for Correspondence: J.D. Humphrey, Ph.D. Department of Biomedical Engineering Malone Engineering Center Yale University 55 Prospect St. New Haven, CT 06520 USA Phone: +1-203-432-6428 jay.humphrey@yale.edu.

Conflicts of Interest
None declared.

years in understanding the mechanics, mechanobiology, and pathophysiology of AAAs (Vorp, 2007; Humphrey and Holzapfel, 2012). One of the most conspicuous early changes in the aneurysmal wall is loss of functional elastic fibers. These fundamental structural constituents endow the wall with diverse mechanical and biological behaviors, including significant distensibility, recoil, and resilience. Several studies have examined effects associated with the loss of elastin (the primary component of elastic fibers) by exposing the infrarenal aorta to pancreatic elastase, an enzyme that degrades elastin (e.g., Anidjar et al., 1990; Pyo et al., 2000; Thompson et al., 2006; Ailawadi et al., 2009; Goergen et al., 2011). Hence, we now understand much more about the sequence of changes in morphology, histology, cell biology, and hemodynamics in the development of model AAAs, including the particularly important role of inflammation. There has been surprisingly little attention to the wall mechanics, however, which is a fundamental determinant of many of the mechanobiological responses that govern the natural history of AAAs as well as the stress and strength that dictate rupture potential. In this study, we present the first biaxial mechanical data and nonlinear constitutive descriptor of the mouse infrarenal aorta immediately after the removal of intramural elastin via an in vitro intraluminal exposure to elastase. These results provide an important characterization of “upper-bound” changes in wall properties due to the near complete loss of elastin, and thereby should help us understand subsequent growth and remodeling of the aortic wall in the in vivo elastase-infused mouse model of AAA.

Methods

Specimen Preparation

Animal care and use was approved by the Texas A&M University Institutional Animal Care and Use Committee and followed our prior methods (cf. Eberth et al., 2009; Collins et al., 2011; Ferruzzi et al., 2011a). The infrarenal abdominal aorta was excised from 8 to 12 week old male wild-type mice immediately following euthanasia, which was accomplished via an overdose of sodium pentobarbital. Specimens were trimmed of excess perivascular tissue, cannulated using custom glass pipettes, and secured to the cannulae using 6-0 silk suture. Branches were either ligated with suture or occluded using microspheres to enable the specimen to be pressurized when mounted in the testing device, which is described elsewhere (Gleason et al., 2004). The testing chamber was filled with a Dulbecco's phosphate-buffered physiological solution containing calcium chloride (Invitrogen, Inc.) and maintained at 37°C.

Mechanical Testing

Initial unloaded dimensions were recorded using a video-microscope, after which the specimen was acclimated to the testing environment for 15 minutes at a distending pressure of 80 mmHg and the approximate in vivo axial stretch (~50% extension based on the cross-over point in axial force – length tests; see Collins et al., 2011). The specimen was then preconditioned via 3 cycles of pressurization from 10 to 140 mmHg at the same axial stretch. Unloaded dimensions were measured again, this time at a pressure of 5 mmHg to avoid possible collapse of the vessel; the increase in dimensions relative to those prior to acclimation and preconditioning was typically negligible. Pressure-diameter testing consisted of cyclic pressurization from 10 to 140 mmHg while maintaining the axial stretch at its in vivo value and then at ± 5% of this value. Axial force-length testing consisted of cyclic loading from 0 to 1.5 g while maintaining pressure constant at 60, 100, and 140 mmHg.

Similar to Ferruzzi et al. (2011a), 3 ml of an elastase-containing solution (having a concentration of 9.5 U of elastase per ml of solution, which contained calcium chloride at

the same concentration as the testing solution) was delivered intraluminally at 100 mmHg and allowed to take effect for 30 minutes at 37°C. The associated increase in outer diameter typically reached a near steady state within 20 minutes. Following the 30 minute exposure, the elastase solution was washed out and replaced with the testing solution. New values of unloaded diameter and length were then recorded and a new "in vivo" stretch was indentified from cyclic axial force – length tests as the value of stretch at which force changed little with increasing pressure. The cyclic pressurization tests were repeated over 10 to 140 mmHg at the new in vivo stretch as well as at 5% above this stretch. Pilot tests revealed that data from tests performed at 5% below the new in vivo stretch were generally not useful because the force remained at or below zero, which is an indicator of either impending bending or bending.

Constitutive Modeling

The biaxial data were converted to mean circumferential and axial Cauchy stresses and stretches using standard formulae (Humphrey, 2002), as, for example, for stress

$$t_{\theta\theta}^{exp}=\frac{P^{exp}a}{h},\quad t_{zz}^{exp}=\frac{f^{exp}}{\pi h\,(2a+h)}, \tag{1}$$

where a is the inner radius in any loaded state and h is the associated thickness of the wall. Following our prior methods (Gleason et al., 2004; Eberth et al., 2009; Collins et al., 2011), the former was inferred from on-line measurements of outer diameter and mean values of wall volume (denoted by an over-bar) based on the assumption of isochoric motions in response to transient loading. For example, letting the undeformed outer and inner radii be denoted by B and A and the undeformed length by L, then

$$V=\pi\left(B^2-A^2\right)L,\quad a=\sqrt{b^2-\overline{V}/(\pi l)}, \tag{2}$$

which in turn allowed wall thickness to be computed easily ($h = b – a$), where b is the on-line measured deformed outer radius. The applied axial force on the artery was computed as $f^{exp}=f_T^{exp}+\pi a^2\,P^{exp}$, where f_T^{exp} is measured by the force transducer and P^{exp} is measured by the pressure transducer.

We used a 2-D "four-fiber family" hyperelastic constitutive model to quantify the loading portion of the biaxial data. This model has proven useful in capturing mechanical responses by diverse mouse arteries (Gleason et al., 2008; Eberth et al., 2009; Wan et al., 2010; Collins et al., 2011; Ferruzzi et al., 2011a). The associated strain-energy function is given by

$$W=\frac{c}{2}\,(I_C-3)+\sum_{k=1}^{4}\frac{c_1^k}{4c_2^k}\left(\exp\left[c_2^k\left(\left(\lambda^k\right)^2-1\right)^2\right]-1\right) \tag{3}$$

where

$$I_C=\lambda_r^2+\lambda_\theta^2+\lambda_z^2,\quad \lambda^k=\sqrt{\lambda_\theta^2\sin^2\alpha^k+\lambda_z^2\cos^2\alpha^k}, \tag{4}$$

and α^k is the angle of the k^{th} fiber family with respect to the axial direction in the reference configuration (i.e., $\alpha^1 = 0$, $\alpha^2 = \pi/2$, $\alpha^3 = -\alpha^4 = \alpha$). Best-fit values of the material parameters c, c_1^k, c_2^k were determined via a nonlinear least squares minimization of the error e (using the routine *lsqnonlin* in MATLAB) between the theoretically predicted (*th*) and experimentally inferred (*exp*) applied loads, namely

$$e=\sum_{i=1}^{N}\left[\left(\frac{P^{th}-P^{exp}}{\overline{P}}\right)_i^2+\left(\frac{f^{th}-f^{exp}}{\overline{f}}\right)_i^2\right], \quad (5)$$

where N is the total number of data points (i.e., equilibrium configurations) for all experimental protocols combined separately for each specimen and the over-bar denotes the overall average value of the experimental measurements. The constrained minimization procedure enforced the physical constraints that $c, c_1^k, c_2^k \geq 0$ and $0 \leq \alpha \leq \pi/2$ due to the symmetry of the diagonal fibers. It is noted that opening angles were not measured due to the use of a 2-D constitutive approach, which cannot incorporate such information.

Exposure to Collagenase

Results from Fonck et al. (2007) and Ferruzzi et al. (2011a) suggest that structural contributions of elastin and collagen to overall wall stiffness are highly coupled. Hence, to explore further the hypothesis that collagen resists some of the elastin-mediated recoil when arteries are unloaded, we also exposed a separate group ($n = 7$) of aortic specimens to 1035 U/ml of collagenase for 120 minutes at 37°C. Because collagenase tends to cause arteries to leak under pressurization, we merely measured the time course (at 0, 10, 20, 30, 45, 60, 90, and 120 minutes) of changes in unloaded dimensions following exposure to collagenase rather than performing biaxial tests.

Histology

All vessels were fixed in 4% formalin in an unloaded state for 1 hour, immersed in cryoprotectant (30% sucrose) overnight, placed in optimum cutting temperature medium in 2-methylbutane cooled with liquid nitrogen, and stored at -80°C. Frozen samples were sectioned at 5 μm and stained with Verhoeff-Van Gieson (VVG) to identify elastin.

Statistics

Geometric data for native and elastase-treated vessels were compared using an unpaired t-test, with $p < 0.01$ considered significant.

Results

Data were qualitatively consistent across the $n = 6$ specimens used as controls and the $n = 5$ specimens exposed to elastase (overall for mice 9.8 ± 0.9 weeks of age and 23.4 ± 1.6 g). The most notable changes resulting from intraluminal exposure to elastase were a marked increase in diameter, decrease in wall thickness, decrease in the “in vivo” axial stretch, and an extreme circumferential stiffening (Table 1; Figures 1 and 2). In particular, noting the different scales in the two panels, Figure 2 reveals that the dramatic changes in mechanical behavior were biaxial as evidenced by the marked rightward shift of the pressure-diameter curve at a lower axial extension following exposure to elastase. Figures 2 and 3 also show representative fits of the constitutive model to pressure-diameter and pressure-force data; for increased clarity in these plots, the data were culled from the original that were used in the nonlinear regressions. The model described the native behavior better than it did the elastase-treated behavior, particularly for the axial direction (e.g., overall errors in the nonlinear regression were $e_{\text{native}} = 8.69 \pm 5.83$ and $e_{\text{elastase}} = 94.56 \pm 76.93$). Nevertheless, best-fit values of the material parameters (Table 2) provided reasonable predictions of the circumferential stress – stretch behavior for both sets of data (Figure 4), which highlighted the extreme loss of distensibility and associated stiffening following exposure to elastase that is reminiscent of aneurysms (cf. Ferruzzi et al., 2011b).

VVG staining confirmed that the dramatic elastase-induced changes in both geometry (e.g., 1.34 ± 0.32 fold increase in unloaded outer diameter and 1.24 ± 0.13 fold increase in unloaded length, which contributed to the decrease in the in vivo axial stretch from 1.49 ± 0.16 to 1.06 ± 0.04; Table 1) and mechanical behavior (Table 2; Figures 2 and 3) were due primarily to a near complete loss of elastin (Figure 5). Finally, Figure 6 shows the time course of changes in unloaded diameter and axial length for the specimens exposed to collagenase over 120 minutes. Note the comparable (6 to 7%) decrease in both diameter and length, with results tending to steady state values after 60 minutes. Collectively, these findings of comparable changes in the circumferential and axial directions were consistent with a nearly isotropic contribution of elastin to the mechanical behavior.

Discussion

AAAs typically present in older men, but also older women. Extreme aging markedly reduces the structural integrity and biological function of elastin (O'Rourke and Hashimoto, 2007), yet an additional nearly complete focal loss of elastin seems to be necessary for the development or enlargement of an aneurysm (He and Roach, 1994). Although it is not yet known what precipitates this additional loss of elastin, there is a pressing need to understand its effects on the mechanics of the infrarenal aorta. This study appears to be the first to investigate acute changes in the biaxial mechanical behavior of the mouse infrarenal aorta due to a nearly complete loss of intramural elastin. The observed changes in geometry, microstructure, and mechanical properties were qualitatively similar, however, to those reported for the effects of elastase on other arteries from various species. For example, Dobrin et al. (1984), Fonck et al. (2007), and Ferruzzi et al. (2011a) also reported that elastase causes a dramatic dilatation, especially at low pressures, and a marked circumferential stiffening of common carotid arteries from dogs, rabbits, and mice, respectively. Whereas Fonck and colleagues reported that the elastase did not alter the overall amount of fibrillar collagen within the wall, Ferruzzi and colleagues suggested that thin (possibly type III) collagen fibers may be affected. Nevertheless, the primary effect on the wall has consistently been ascribed to the dramatic decrease in elastin (cf. Figure 5).

Recall that the isotropic neo-Hookean contribution to the stored energy function (first term in equation 3) is motivated by the presence of structurally competent elastin (Ferruzzi et al., 2011a,b). Our constitutive model captured the near total loss of elastin via an orders of magnitude decrease in the best-fit value of the associated parameter c (Table 2), which reduced on average from 8.95 kPa for the native infrarenal aorta to 1.69×10^{-5} kPa following exposure to elastase. Parameters associated with the circumferential family of fibers (thought to be dominated by types I and III collagen) also changed notably following exposure to elastase: $c_1^2 > c_2^2$ for the native response, but $c_1^2 < c_2^2$ for the response following exposure to elastase. The relative magnitudes of these two parameters dictate the “rate” of stiffening revealed by the stress – stretch response and thus reflect the dramatic decrease in distensibility and increase in circumferential stiffness seen in Figure 4. As discussed by Ferruzzi et al. (2011a), and consistent with conclusions by Fonck et al. (2007), parallel changes in values of the elastin- and collagen-associated parameters suggest a strong mechanical coupling between these two constituents. Indeed, nonlinear optical microscopic images reported by Ferruzzi and colleagues support the hypothesis that elastin and collagen exist at different pre-stretches within the normal arterial wall. When the wall is unloaded, the elastin attempts to recoil elastically more than does the collagen and thus it tends to compress the collagen (which is probably facilitated by interactions with proteoglycans); this compression introduces an undulation in the collagen that facilitates a more gradual stiffening of the native wall (Figure 4). Loss of elastin thus diminishes the undulation of

collagen and thereby results in the observed decrease in both distensibility and extensibility (at a larger diameter and length) as well as the increased stiffness (Figures 2 and 4).

The hypothesis that competent elastin influences the undulation, and hence stiffness, of collagen is consistent with a report by Zeller and Skalak (1998) on residual stresses in arteries. Using elastase and collagenase to delineate effects of elastic and collagen fibers on the residual stresses in unloaded segments of arteries, they concluded that elastin is in tension and collagen is in compression within the unloaded wall. Although exposure to collagenase results in leaky vessels that are not amenable to careful biaxial testing (cf. Dobrin et al., 1984), we used collagenase to test further the hypothesis that collagen resists the recoil of competent elastic fibers. That is, we hypothesized that loss of collagen should allow elastin in an unloaded vessel to recoil further and thereby decrease the unloaded dimensions. Results presented in Figure 6 support this hypothesis. We suggest that these results from the collagenase study complement those obtained via nonlinear optical microscopy by Ferruzzi et al. (2011a). Nonlinear optical microscopy was not employed herein for it was not expected to yield results qualitatively different from those reported previously on carotid arteries.

Whereas the present results reveal, for the first time, changes in mouse aortic structure and biaxial mechanical properties due to the nearly complete acute loss of intramural elastin, there are important differences between our in vitro results and the aforementioned in vivo mouse models that are based on the infusion of elastase in the infrarenal aorta. We used a 30-minute intraluminal exposure to 9.5 U/ml of elastase, which is consistent with prior in vitro studies on other vessels (Dobrin et al., 1984; Fronck et al., 2007; Ferruzzi et al., 2011a) as well as the first in vivo study in rats (Andijar et al., 1990). In contrast, most recent in vivo studies in mice use 5-minute intraluminal exposures to 0.5 to 1.5 U/ml of elastase (cf. Pyo et al., 2000; Aliwadi et al., 2009). Such exposures result in modest initial changes to the elastic lamellae and associated modest initial changes in diameter (30-60%), which actually appear to be independent of the proteolytic activity of the elastase (van Vickle-Chavez et al., 2006). Subsequent in vivo enlargement of the lesion tends to occur over many days and to include a progressive loss of elastin (see Figure 1 in van Vickle-Chavez et al., 2006). Progressive changes in morphology, histology, and cell biology result in large part from inflammatory processes that are presumably initiated by the initial exposure to elastase, with different cell types playing important roles (e.g., neutrophils, mast cells, and macrophages; cf. Eliason et al., 2005 and Sun et al., 2009). One advantage of our study is that it delineates effects on aortic geometry and biaxial mechanical behavior due to the near complete loss of elastin without the confounding effects of collagen remodeling that necessarily occurs in vivo in the mouse as the elastin is lost. Of course, to obtain a more complete understanding of the evolving mechanical properties of the aneurysmal wall as well as the contributions due to elastin, collagen, and other structural constituents, there is now a need to perform comparable biaxial tests on specimens excised at multiple times during the development of these lesions in vivo. The present results are thus but a necessary first step toward this ultimate goal.

In conclusion, the observed damage to or degradation of elastic fibers in human AAAs (cf. Humphrey and Holzapfel, 2012) motivated the in vivo elastase-infusion model in rodents (Anidjar et al., 1990) that remains popular (e.g., Ailawadi et al., 2009; Goergen et al., 2011). Although the associated mechanisms are not understood fully, much has been learned using this model. We suggest that, in combination with continued molecular and cellular studies, computational models of growth and remodeling of the elastase-damaged aortic wall (cf. Wilson et al., 2012) may help us understand better the evolution of AAAs in this mouse model and ultimately in humans, and the present data represent another important step in that direction.

Acknowledgments

This research was supported, in part, by a grant from the NIH (R01 HL105297). We also thank a talented undergraduate student at Texas A&M, Jacyln Boone, who assisted with the experiments.

References

Ailawadi G, Moehle CW, Pei H, Walton SP, Yang Z, Kron IL, Lau CL, Owens GK. Smooth muscle phenotypic modulation is an early event in aortic aneurysms. J Thorac Cardiovasc Surg. 2009; 138:1392–1399. [PubMed: 19931668]

Anidjar S, Salzmann JL, Gentric D, Lagneau P, Camilleri JP, Michel JB. Elastase-induced experimental aneurysms in rats. Circulation. 1990; 82:973–981. [PubMed: 2144219]

Collins MJ, Bersi M, Wilson E, Humphrey JD. Mechanical properties of surarenal and infrarenal abdominal aorta: implications for mouse models of aneurysms. Med Eng Phys. 2011 doi:10.10.16/j.medengphy.2011.06.003.

Dobrin PB, Canfield TR. Elastase, collagenase, and the biaxial elastic properties of dog carotid artery. Am J Physiol. 1984; 247:H124–131. [PubMed: 6331204]

Eberth JF, Taucer AI, Wilson E, Humphrey JD. Mechanics of carotid arteries in a mouse model of Marfan Syndrome. Ann Biomed Engr. 2009; 37:1093–1104.

Eliason JL, Hannawa KK, Aliwadi G, Shinha I, Ford JW, Deogracias MP, Roelifs KJ, Woodrum DT, Ennis TL, Henke PK, Stanley JC, Thompson RW, Upchurch GR. Neutrophil depletion inhibits experimental abdominal aortic aneurysm formation. Circulation. 2005; 112:232–240. [PubMed: 16009808]

Ferruzzi J, Collins MJ, Yeh AT, Humphrey JD. Mechanical assessment of elastin integrity in fibrillin-1 deficient carotid arteries: implications for Marfan syndrome. Cardiovasc Res. 2011a in press.

Ferruzzi J, Vorp DA, Humphrey JD. On constitutive descriptors of the biaxial mechanical behavior of human abdominal aorta and aneurysms. J R Soc Interface. 2011b; 8:435–350. [PubMed: 20659928]

Fonck E, Prod'hom G, Roy S, Augsburger L, Rüfenacht DA, Stergiopulos N. Effect of elastin degradation on carotid wall mechanics as assessed by a constituent-based biomechanical model. Am J Physiol. 2007; 292:H2754–H2763.

Gleason RL, Gray SP, Wilson E, Humphrey JD. A multiaxial computer-controlled organ culture and biomechanical device for mouse carotid arteries. J Biomech Engr. 2004; 126:787–795.

Gleason RL, Dye WW, Wilson E, Humphrey JD. Quantification of the mechanical behavior of carotid arteries from wild-type, dystrophin-deficient, and sarcoglycan-delta knockout mice. J Biomech. 2008; 41:3213–3218. [PubMed: 18842267]

Goergen CJ, Azuma J, Barr KN, Magdefessel L, Kallop DY, Goginrni A, Grewall A, Weimer RM, Connolly AJ, Dalman RL, Taylor CA, Tsao PS, Greve JM. Influences of aortic motion and curvature on vessel expansion in murine experimental aneurysms. Arterioscler Thromb Vasc Biol. 2011; 31:270–279. [PubMed: 21071686]

He CM, Roach MR. The composition and mechanical properties of abdominal aortic aneurysms. J Vasc Surg. 1994; 20:6–13. [PubMed: 8028090]

Humphrey, JD. Cardiovascular Solid Mechanics: Cells, Tissues, and Organs. Springer-Verlag, NY; New York: 2002.

Humphrey JD, Holzapfel GA. Mechanics, mechanobiology, and modeling human abdominal aorta and aneurysms. J Biomech. 2011 (accepted).

O'Rourke MF, Hashimoto J. Mechanical factors in arterial aging: A clinical perspective. J Am Coll Cardiol. 2007; 50:1–13. [PubMed: 17601538]

Pyo R, Lee JK, Shipley JM, Curci JA, Mao D, Ziporin SJ, Ennis TL, Shapiro SD, Senior RM, Thompson RW. Targeted gene disruption of matrix metalloproteinase-9 (gelatinase B) suppresses development of experimental abdominal aortic aneurysms. J Clin Invest. 2000; 105:1641–1649. [PubMed: 10841523]

Sun J, Zhang J, Lindholt JS, Sukhova GK, Liu J, He A, Abrink M, Pejler G, Stevens RL, Thompson RW, Ennis TL, Gurish MF, Libby P, Shi G-P. Critical role of mast cell chymase in mouse abdominal aortic aneurysm formation. Circulation. 2009; 120:973–982. [PubMed: 19720934]

Thompson RW, Curci JA, Ennis TL, Mao D, Pagano MB, Pham CT. Pathophysiology of abdominal aortic aneurysms: insights from the elastase-induced model in mice with different genetic backgrounds. Annl NY Acad Sci. 2006; 1085:59–73.

Van Vickle-Chavez SJ, Tung WS, Absi TS, Ennis TL, Mao D, Cobb JP, Thompson RW. Temporal changes in mouse aortic wall gene expression during the development of elastase-induced abdominal aortic aneurysms. J Vasc Surg. 2006; 43:1010–1020. [PubMed: 16678698]

Vorp DA. Biomechanics of abdominal aortic aneurysm. J Biomech. 2007; 40:1887–1902. [PubMed: 17254589]

Wan W, Yanagisaw H, Gleason RL. Biomechanical and microstructural properties of common carotid arteries from fibulin-5 null mice. Annl Biomed Engr. 2010; 38:3605–3617.

Wilson J, Baek S, Humphrey JD. Importance of initial aortic properties on the evolving regional anisotropy, stiffness, and wall thickness of human abdominal aortic aneurysms. 2011 (submitted).

Zeller PJ, Skalak TC. Contribution of individual structural components in determining the zero-stress state in small arteries. J Vasc Res. 1998; 35:8–17. [PubMed: 9482691]

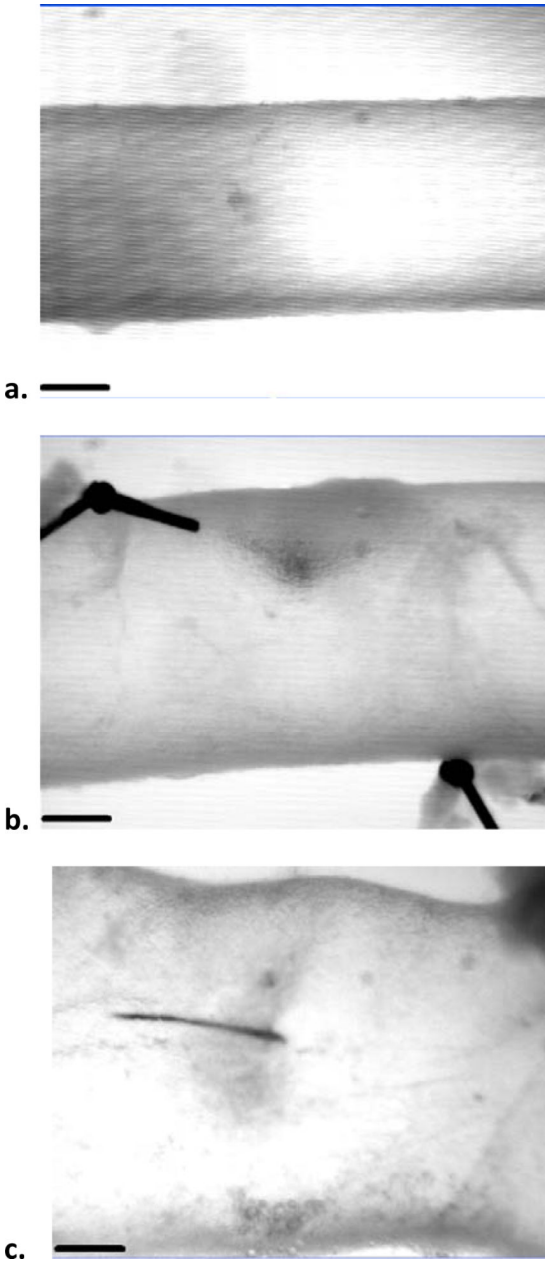

Figure 1.
Video-microscope images of the infrarenal aorta mounted within the test device at 100 mmHg and its normal in vivo axial stretch before (a) and after (b and c) exposure to 9.5 U/ml of elastase for 30 minutes. The dramatic acute dilatation was typically non-uniform and highly variable, with a mean value of 56% (panels b and c show examples of an ~34% dilatation and an unusually high 92% dilatation, respectively). The scale bar is 200 microns.

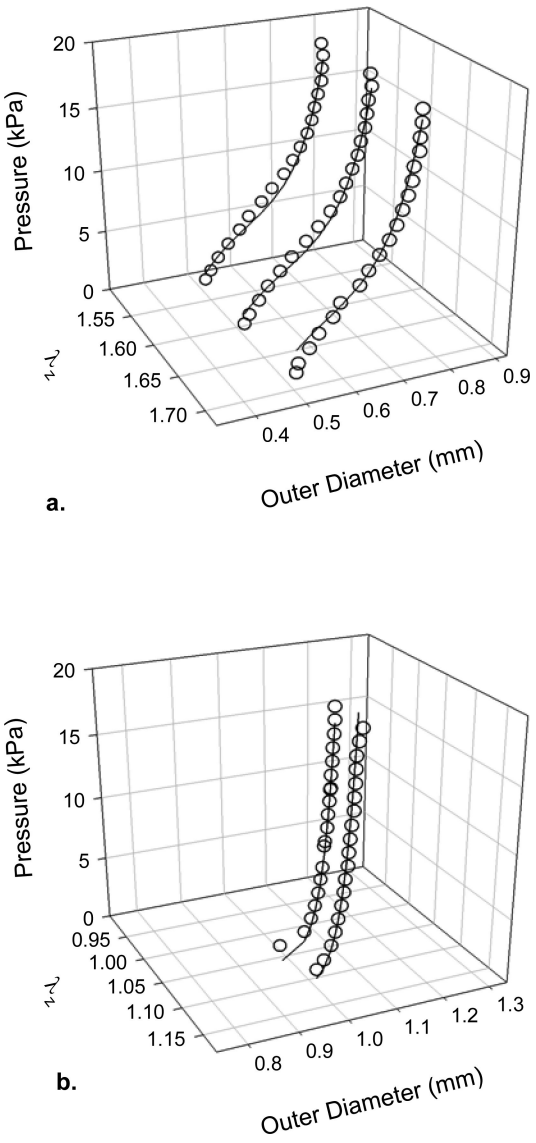

Figure 2.

Pressure-diameter data (open symbols) collected at multiple values of axial stretch before (a) and after (b) exposure to elastase. The elastase caused a dramatic rightward shift in the pressure-diameter response and much lower values of axial stretch (note the different scales). The solid lines show the fit to data with our constitutive relation. The data were culled for clarity when plotted.

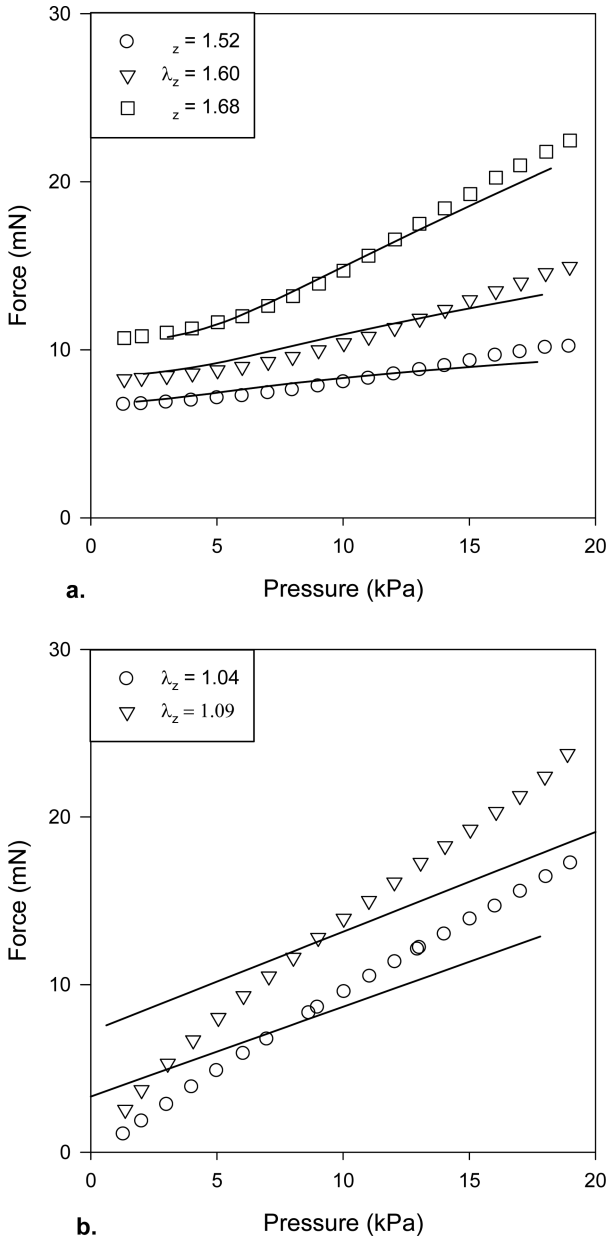

Figure 3.

Force-pressure data (open symbols) collected during cyclic pressurization tests at multiple values of axial stretch before (a) and after (b) exposure to elastase. The solid lines again show the fit to the data, which were culled simply for clarity when plotted.

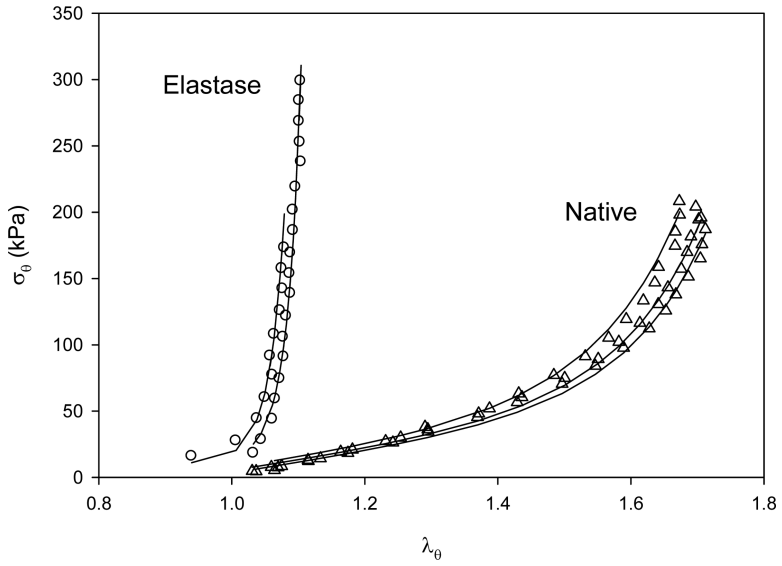

Figure 4.
Comparison of circumferential Cauchy stress-stretch behaviors (symbols) for representative native and elastase-treated infrarenal aorta and the associated predictions (solid curves) based on the equation 3 and best-fit values of parameters listed in Table 2. Note the marked decrease in circumferential distensibility and increase in circumferential stiffness following exposure to elastase.

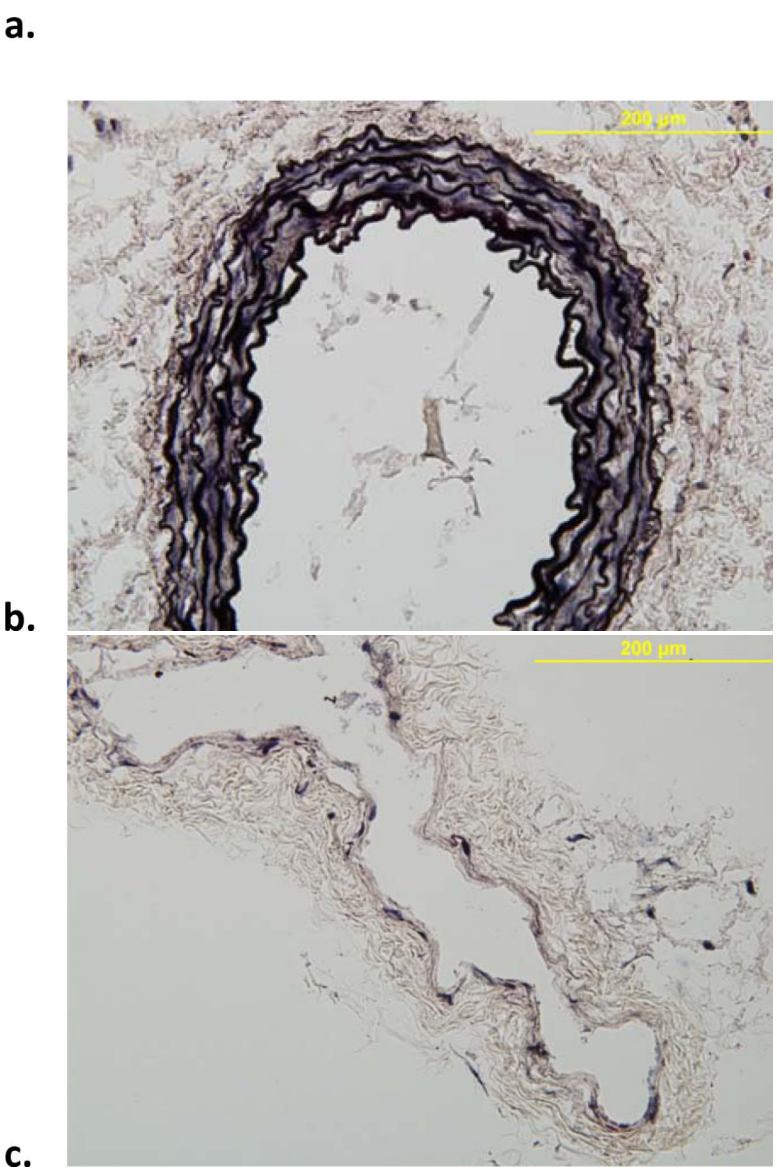

Figure 5.
Representative VVG-stained histological images (showing elastin in black) of mouse infrarenal aorta before (a) and after (b) exposure to elastase. The elastase resulted in a near complete loss of elastin and extreme thinning of the wall; note that the normal wall consists of 3 to 5 elastic lamellae and that the specimens were fixed in unloaded configurations.

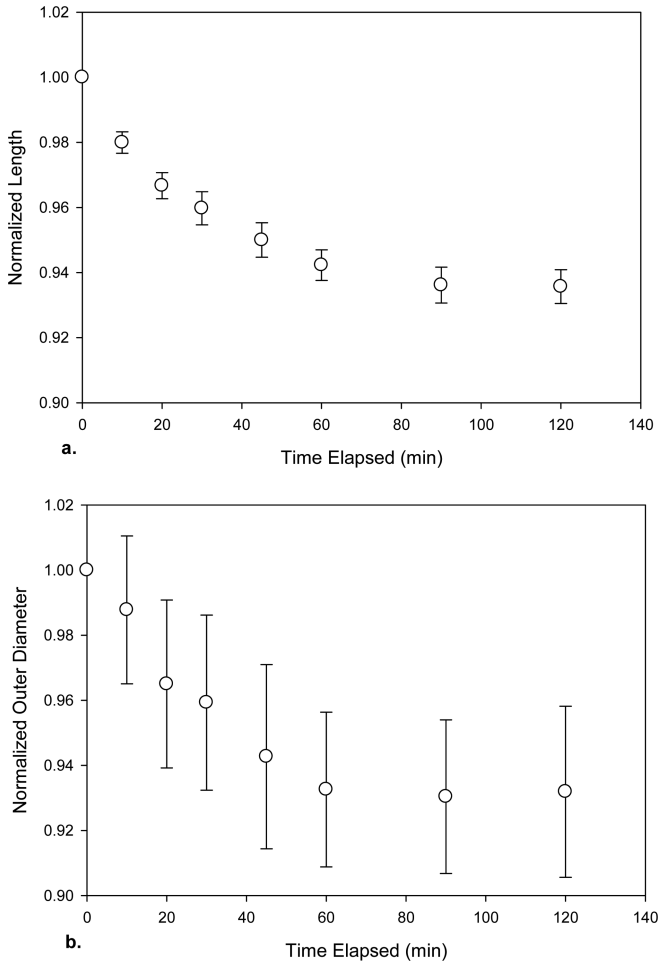

Figure 6.

Time course of changes in geometry following exposure of $n = 7$ unloaded arteries to 1035 U/ml of collagenase: overall length (a) and outer diameter at multiple locations along the length (b). Note the similar (6-7%) decreases in the two directions. The larger standard deviations in the diameter measurements resulted from the fraying and loss of adventitial collagen.

Table 1

Mean ± standard deviation for relevant data on the unloaded geometry (outer diameter *OD*, thickness H, and overall length *L*), in vivo axial stretch (λ_z^{iv}), and pressurized inner radius *a* and wall thickness *h* of the infrarenal aorta before (native) and after (elastase) a 30-minute intraluminal exposure to 9.5 U/ml of elastase. All differences for vessels before and after exposure to elastase were statistically significant at $p < 0.01$ (t-test), as denoted by an *. In addition to the typically reported extreme dilatation under in vivo loading (~56% on average), the unloaded wall thickness decreased ~55% (cf. Figure 4) and the unloaded length increased ~24% due to the elastase.

Vessel	OD* (μm)	H* (μm)	L* (mm)	$\lambda_z^{iv} * (- \; -)$	a* (μm) @ 80 mmHg	h* (μm) @ 80 mmHg
Native (n=6)	537 ± 55	87.2 ± 9.3	3.55 ± 0.75	1.47 ± 0.20	309 ± 28	40.8 ± 8.1
Elastase (n=5)	722 ± 182	39.0 ± 10.5	4.42 ± 0.71	1.06 ± 0.04	482 ± 48	23.8 ± 2.1

Table 2

Best-fit values (mean ± standard deviation) of the parameters in the constitutive relation given in equation 3 for n = 6 control and n = 5 elastase-exposed specimens. As noted by Ferruzzi et al. (2011b), however, median values may provide better estimates of the overall behavior described this constitutive descriptor. Median values following exposure to elastase were c = 6.02 E-07 kPa, c_1^1=154.78 kPa, c_2^1=1.45 E−08, c_1^2=1.69 E−06, c_2^2=0.24, $c_1^{3,4}$=0.60 kPa, $c_2^{3,4}$=3.85, and α = 47.09 degrees.

		AXIAL		CIRCUMFERENTIAL		DIAGONAL		
Vessel	**c (kPa)**	c_1^1**(kPa)**	c_1^2	c_2^1**(kPa)**	c_2^2	$c_1^{3,4}$**(kPa)**	$c_2^{3,4}$	α **(deg)**
Native ± SD	8.95 ± 6.77	8.59 ± 6.18	1.24 ± 2.31	6.54 ± 2.26	0.28 ± 0.22	1.65 ± 1.83	1.86 ± 1.17	34.63 ± 5.75
Elastase ± SD	1.7E-5 ± 3.4E-5	104.74 ± 97.14	0.02 ± 0.03	21.92 ± 35.16	79.78 ± 157.66	32.03 ± 46.61	31.46 ± 61.92	41.42 ± 12.78